University of Szeged
Faculty of Pharmacy
Institute of Pharmaceutical Technology and Regulatory Affairs
Head: Prof. Dr. Ildikó Csóka, Ph.D.

Summary of Ph.D. Thesis

INHALABLE KETOPROFEN NANOCRYSTAL-BASED DRY POWDERS FOR LOCAL AND SYSTEMIC PULMONARY DELIVERY: A PATIENT-CENTRIC APPROACH

By

Heba Banat

Pharmacist

Supervisor:

Prof. Dr. Ildikó Csóka

and

Prof. Dr. Rita Ambrus

SZEGED

2025

University of Szeged
Doctoral School of Pharmaceutical Sciences
Head: Prof. Dr. Judit Hohmann, D.Sc.
Educational Program: Pharmaceutical Technology and Regulatory Science
Head: Prof. Dr. Ildikó Csóla, Ph.D.
Institute of Pharmaceutical Technology and Regulatory Affairs
Supervisor:
Prof. Dr. Ildikó Csóka, Ph.D.
and
Prof. Dr. Rita Ambrus, D.Sc.

Heba Fayez Mahmoud Banat

INHALABLE KETOPROFEN NANOCRYSTAL-BASED DRY POWDERS FOR LOCAL AND SYSTEMIC PULMONARY DELIVERY: A PATIENT-CENTRIC APPROACH

Complex Exam Committee:

Head:	**Prof. Dr. Piroska Szabó-Révész**, D.Sc., University of Szeged, Faculty of Pharmacy, Institute of Pharmaceutical Technology and Regulatory Affairs
Members:	**Dr. Gabriella Csóka**, Ph.D., Meditop Pharmaceutical Ltd.
	Dr. Tamás Sovány, Ph.D., University of Szeged, Faculty of Pharmacy, Institute of Pharmaceutical Technology and Regulatory Affairs

Reviewer Committee:

Head:	**Prof. Dr. István Zupkó**, D.Sc., University of Szeged, Faculty of Pharmacy, Institute of Pharmacodynamics and Biopharmacy
Reviewers:	**Prof. Dr. Noémi Csaba**, Ph.D., University of Santiago de Compostela, Department of Pharmacology, Pharmacy and Pharmaceutical Technology
	Prof. Dr. Romana Zelko, D.Sc., University of Semmelweis, Faculty of Pharmacy, Institute of Pharmaceutical Management
Secretary:	**Dr. Gerda Szakonyi**, Ph.D., University of Szeged, Faculty of Pharmacy, Institute of Pharmaceutical Analysis
Member:	**Dr. Andrea Vasas**, Ph.D., University of Szeged, Faculty of Pharmacy, Department of Pharmacognosy

Szeged

2025

ABBREVIATIONS

A549	Adenocarcinomic human alveolar basal epithelial cells
ACI	Andersen cascade impactor
A_m	Surface area of the membrane
ANOVA	Analysis of Variance
API	Active pharmaceutical ingredient
APS	Aerodynamic Particle Sizer
AUC	Area under the curve
BBD	Box-Behnken factorial design
BCS	Biopharmaceutical Classification System
C_A	Concentration of the acceptor phase
C_D	Concentration of the donor phase
CF	Cystic fibrosis
CFBE	Cystic fibrosis bronchial epithelial cells
C_{max}	Maximum concentration
CQAs	Critical Quality Attributes
COX	Cyclooxygenase enzyme
D[0.1]	10% of the volume distribution is below this value
D[0.5]	50% of the volume distribution is below this value
D[0.9]	90% of the volume distribution is below this value
DL	Drug loading
DLS	Dynamic light scattering
DPI	Dry powder inhaler
DSC	Differential scanning calorimetry
EE	Encapulation efficiency
EELV	End-expiratory lung volume
EF	Emitted fraction
F	Relative bioavailability
FBS	Fetal bovine serum
FPF	Fine particle fraction
f_t	Tissue availability
FT-IR	Fourier-Transform Infrared Spectroscopy
G	Tissue damping
GSD	Geometric standard deviation
H	Tissue elastance
HEPES	4-(2-hydroxyethyl)-1-piperazineethanesulfonic acid
HPMC	Hydroxypropyl methylcellulose
ICH	The International Council for Harmonization of Technical Requirements for Pharmaceuticals for Human Use
IVIVC	In vitro-in vivo correlation
IL-6	Interleukin 6
IUPAC	International Union of Pure and Applied Chemistry
k_e	Elimination rate constant
KTP	Ketoprofen
LPS	Lipopolysaccharide

MEM	Minimum Essential Medium
MMAD	Mass median aerodynamic diameter
M_w	Molecular weight
NCA	Nanocrystal agglomerate
NS	Nanosuspension
NSAID	Non-steroidal anti-inflammatory drug
NTA	Nanoparticle Tracking Analysis
OVA	Ovalbumin
P_{app}	Apparent permeability coefficients
PDI	Polydispersity index
PEEP	Positive end-expiratory pressure
PK	Pharmacokinetics
PM	Physical mixture
PS	Particle size
PVA	Polyvinyl alcohol
QbD	Quality by Design
QTPP	Quality Target Product Profile
R_{aw}	Airway resistance
RI	Refractive index
RPMI	Roswell Park Memorial Institute medium
S.D.	Standard deviation
SDS	Sodium dodecyl sulphate
SEM	Scanning electron microscopy
SSA	Specific surface area
t	Time
TEER	Transepithelial electrical resistance
U937	Promonocyte cells
X_c	Crystallinity index
XRPD	X-ray powder diffraction
ZP	Zeta potential
ZrO_2	Zirconium-dioxide
ρ_b	Bulk density
ρ_t	Tapped density

1. Introduction

Pulmonary drug delivery offers a non-invasive route for both local and systemic therapy, leveraging the lungs' large surface area, rich vascularization, and avoidance of first-pass metabolism to enhance bioavailability. Dry powder inhalers (DPIs) are particularly advantageous due to their stability, propellant-free design, and ease of use. While inhaled non-steroidal anti-inflammatory drugs (NSAIDs) have shown promise for treating local lung inflammation, their systemic applications remain underexplored, despite the potential for lower therapeutic doses and reduced systemic side effects compared to oral administration.

NSAIDs are widely used to treat inflammatory conditions, including cystic fibrosis (CF) and acute pain; however, oral administration is limited by gastrointestinal toxicity, poor solubility, and variable bioavailability. Pulmonary delivery could overcome these challenges, yet no inhaled NSAID has been translated into a marketed product. Nanocrystals, as a carrier-free platform (typically 1–1000 nm), offer distinct advantages for pulmonary delivery, including enhanced dissolution, improved mucus penetration, and high drug loading. However, their small size necessitates precise particle engineering to ensure aerodynamic diameters within the optimal range (1–5 μm) for lung deposition.

This work introduces two patient-centric ketoprofen (KTP)-based DPI formulations derived from a unified nanocrystal platform. The first combines KTP with the mucolytic agent mannitol for localized pulmonary therapy, targeting both inflammation and mucus clearance in diseases such as CF. The second leverages nanocrystal engineering for systemic NSAID delivery, aiming to improve bioavailability while minimizing gastrointestinal irritation. Both formulations are designed to simplify treatment regimens and enhance tolerability.

By integrating Quality by Design (QbD) principles with nanocrystal technology, this study advances the development of inhaled NSAIDs through tailored strategies for local and systemic indications. The approach not only addresses current therapeutic gaps but also establishes a framework for repurposing poorly soluble drugs via pulmonary delivery—aligning with regulatory priorities for patient-centric, innovative drug products.

2. Aim of the work

This study proposes a patient-centric strategy for pulmonary drug delivery through the development of two distinct DPI systems derived from a unified KTP nanocrystal platform. One formulation targets local lung inflammation and mucus obstruction in CF, while the other is designed for systemic delivery to enhance bioavailability via the pulmonary route. The overarching aim is to tailor drug formulation to meet different therapeutic needs while aligning with patient expectations for rapid relief, reduced dosing burden, and improved tolerability. The specific objectives are as follows:

A. Nanocrystal dispersion development

I. Formulate and optimize a stable KTP nanosuspension as a versatile intermediate for both local and systemic DPI products, ensuring suitability for downstream powder engineering.

B. Local pulmonary delivery (Anti-inflammatory and mucolytic combination):

II. Establish a rational inhalable combination of KTP and mannitol guided by a QbD approach.

III. Develop the combined dry powder formulation using mini spray-drying with varying mannitol ratios to optimize the combination while maintaining KTP integrity.

IV. Assess the dual functionality of the formulation through evaluation of local efficacy, biocompatibility, and epithelial permeability.

C. Systemic pulmonary delivery (Nanocrystal-engineered DPI):

V. Optimize the nano spray-drying process parameters, with a factorial design, to produce nanocrystal-engineered powders suitable for deep lung deposition and systemic absorption.

VI. Investigate the influence of excipients (mannitol and leucine) on aerosol performance, biocompatibility, and cellular diffusion.

VII. Assess the pharmacokinetic profile of the inhaled nanocrystal formulation compared to the oral route, alongside tolerability and safety in ovalbumin-sensitized rats.

D. Stability evaluation:

VIII. Determine the physicochemical stability of both DPI systems under accelerated storage conditions, ensuring maintenance of performance-critical attributes.

3. Materials

3.1. Active pharmaceutical ingredient

KTP, with the IUPAC name *2-(3-benzoylphenyl)propanoic acid*, was used as the primary API (TCI Chemicals, Shanghai, China). KTP is an NSAID classified under Biopharmaceutical Classification System (BCS) class II, with poor water solubility (51 mg/L at 22 °C) and high permeability (log P = 3.12).

3.2. Excipients

Poly-vinyl-alcohol (PVA, Mw ~27,000 g/mol; Aldrich Chemistry, Darmstadt, Germany), and sodium dodecyl sulfate (SDS, Mw 288.38 g/mol; VWR Chemicals, Leuven, Belgium) were utilized as stabilizers in the nanosuspension preparation. D-mannitol (Mw 182.17 g/mol; Molar Chemicals Ltd., Budapest, Hungary) was incorporated as a secondary API in the spray-dried formulation intended for local pulmonary delivery, owing to its mucolytic activity. Additionally, its role as a formulation excipient was evaluated in the nano spray-dried formulations intended for systemic delivery. L-leucine (Mw 131.17 g/mol; AppliChem GmbH, Darmstadt, Germany) was included as a dispersibility enhancer.

4. Methods

4.1. Production of the nanosuspension by wet milling

A KTP-containing nanosuspension (KTP-NS) was developed using a two-step process. First, KTP particles were dispersed in an aqueous stabilizing solution and homogenized using an Ultra-Turrax homogenizer (T-25, IKA-Werke, Germany) at 17,000 rpm for 10 minutes. The resulting pre-suspension was then subjected to wet media milling using a planetary ball mill (Retsch PM 100 MA, Retsch GmbH, Haan, Germany), with 20.00 g of 0.3 mm zirconium dioxide (ZrO_2) beads at 400 rpm for 90 minutes in a 50 mL milling chamber. The final drug concentration in the nanosuspension was 10% (w/v), and samples were diluted as required for further analysis or processing.

4.1.1. Selection of the stabilizers

Three different stabilizers were evaluated, each tested at three concentrations: i) HPMC at 0.25, 0.50, and 1.00% (w/v); ii) PVA at 1.00, 2.50, and 5.50% (w/v); iii) Poloxamer 188 at 0.20, 0.50, and 1.00% (w/v). SDS was included in all formulations at a fixed concentration of 0.10% (w/v). The resulting nanosuspensions were characterized in terms of particle size, and the most effective stabilizer was selected for further investigations.

4.1.2. Particle size analysis of the nanosuspension

4.1.2.1. Dynamic light scattering (DLS)

Particle size (PS), polydispersity index (PDI), and zeta potential (ZP) of KTP-NS were measured using a Zetasizer Nano ZS (Malvern Instruments, UK). Each sample was analyzed in triplicate, and the average values were reported.

4.1.2.2. Nanoparticle size tracking analysis (NTA)

The particle size distribution of KTP-NS was determined using the NanoSight NS3000 (Malvern Instruments, UK). Particle size metrics included D[0.1], D[0.5], and D[0.9], while the size distribution span was calculated according to Equation 1.

$$\text{Span} = \frac{\text{D}[0.9] - \text{D}[0.1]}{\text{D}[0.5]} \quad (1)$$

4.1.3. Stability of the nanosuspension

To assess the stability of the KTP-NS prior to the drying process, a short-term stability study was conducted. The nanosuspension was stored at refrigeration temperature (+4 °C) and evaluated for particle size and distribution at predefined time intervals.

4.2. Inhalable ketoprofen-mannitol combination powder: Local delivery

4.2.1. Application of QbD to define the rationale for novel powder combinations

The QbD framework was applied during the pre-formulation design (zero phase) to rationally select and justify the components of the novel inhalable combination. A flowchart was used to outline key challenges in CF and highlight the need for combination inhaled therapies. To further identify factors affecting product quality, an Ishikawa (fishbone) diagram was developed, helping to pinpoint variables influencing Critical Quality Attributes (CQAs). Based on this analysis, a Quality Target Product Profile (QTPP) was defined.

4.2.2. Formulation of combined DPI using mini spray drying

To achieve local pulmonary targeting, combination powders were prepared using Mini Spray Dryer B-19 (Büchi, Flawil, Switzerland). Spray drying parameters were set as follows: inlet temperature, 90 °C; aspirator setting, 80%; pump rate, 2%; and air flow rate, 600 L/h. The KTP-NS was diluted to 1% (w/v), and mannitol—used for its mucolytic properties—was incorporated at varying concentrations to determine the highest amount that could be included without adversely affecting the integrity of KTP. Four spray-dried formulations were prepared with mannitol-to-KTP mass ratios of 0, 0.5:1, 1:1, and 2:1, and were named F0, F0.5, F1, and F2 according to their mannitol content. Additionally, a

dispersity enhancer (leucine) was included in all formulations at a fixed mass ratio of 1:1 (leucine:KTP).

4.3. Inhalable ketoprofen nanocrystal-based dry powder: Systemic delivery

4.3.1. Optimization of nano spray-drying parameters

Nano Spray Dryer B-90 HP (Büchi, Flawil, Switzerland) equipped with a medium nebulizer was used to engineer KTP-containing nanocrystal agglomerates (NCAs) for targeting systemic effect. The Box-Behnken factorial design (BBD) was employed to optimize the drying parameters, assisted by TIBCO Statistica® 13.4 (Statsoft Hungary, Budapest, Hungary) for experimental design generation. The effect of three independent factors (pump rate (%), inlet temperature (°C), and feed concentration (% w/v)) on the dependent variables (D[0.5], span, and yield) was investigated at three levels. Temperature was studied at 90, 100, and 110 °C, feed concentration was evaluated at 10% 5% and 2.5% (w/v), while pump percentage was assessed at 10%, 30%, and 50%.

4.3.2. Incorporation of mannitol and/or leucine as excipients

Using optimized nano spray dryer parameters, we evaluated the impact of excipients—mannitol (K1M), leucine (K1L), their combination (K1ML), and the absence of excipients (K1)—on the properties of NCAs for pulmonary delivery (Table 1).

Table 1: Samples annotation, composition and concentration*

Sample	KTP (% w/v)	Mannitol (% w/v)	Leucine (% w/v)
K1	5.00	0	0
K1M	2.50	2.50	0
K1L	2.50	0	2.50
K1ML	2.50	1.25	1.25

*The concentrations of the samples were maintained to meet the optimized feed concentration of 5% w/v, as determined by the factorial design study.

4.4. Powder characterization

4.4.1. Particle size and density

Spray-dried powders were re-dispersed in deionized water and analyzed for PS, PDI, and ZP using a Zetasizer Nano ZS (Malvern Instruments, UK). Also, laser diffraction was used to assess the particle size and distribution of the spray-dried samples with a Mastersizer Scirocco 2000 device (Malvern Instruments Ltd., UK). A dry dispersion unit was employed with 0.5–1.0 g of powder placed in the feeding tray. Parameters including D[0.5], and specific surface area (SSA) were evaluated, and the span was calculated as previously defined (Equation 1). Furthermore, spray-dried samples were evaluated for tapped (ρt) and bulk (ρb) densities using an Engelsmann Stampfvolumeter (Ludwigshafen, Germany).

4.4.2. Drug loading, encapsulation efficiency and yield

To calculate drug loading (DL) and encapsulation efficiency (EE), a measured amount of the spray-dried samples was dissolved in 50% (v/v) methanol and analyzed by UV/VIS Spectrophotometer (ATI-Unicam, Cambridge, UK) at 258 nm (Equations 2 and 3). Moreover, percentage yields of dry powder collected after spray drying was calculated (Equation 4).

$$\text{DL}\ (\%) = \frac{\text{Weight of the drug}_{(\text{measured})}}{\text{Total weight of the dry powder}_{(\text{drug + excipients})}} \times 100\% \quad (2)$$

$$\text{EE}\ (\%) = \frac{\text{Weight of the drug}_{(\text{measured})}}{\text{Initial weight of the drug added}} \times 100\% \quad (3)$$

$$\text{Yield}\ (\%) = \frac{\text{Weight of dry powder collected}_{(\text{after spray drying})}}{\text{Weight of the initial solid composition}_{(\text{before spray drying})}} \times 100\% \quad (4)$$

4.4.3. Morphology

The morphology was analysed using a scanning electron microscope (SEM) (Hitachi Scientific Ltd. in Tokyo, Japan). Also, the particle size was calculated using ImageJ 1.53e software, with measurements taken from 50 to 100 particles per sample.

4.4.4. Solid-state analysis

Differential Scanning Calorimetry (DSC) and Thermogravimetric Analysis (TGA) were performed using Mettler Toledo DSC 821e and TGA/DSC1 systems, respectively, equipped with STARe software v9.3 (Mettler Inc., Schwerzenbach, Switzerland). X-ray Powder Diffraction (XRPD) was carried out using a BRUKER D8 Advance diffractometer (Bruker AXS GmbH, Germany). Crystallinity index (Xc) was calculated using OriginPro v9.6.5.1, referencing pure KTP as 100% crystalline (Equation 5).

$$\text{Xc}\ (\%) = \frac{\text{A crystalline}}{\text{A crystalline} + \text{A amorphous}} \times 100\% \quad (5)$$

Fourier-Transform Infrared Spectroscopy (FT-IR) was performed using an AVATAR 330 FT-IR spectrometer (Thermo Fisher Scientific, USA). Spectra were recorded from 4000 to 400 cm^{-1} at 4 cm^{-1} resolution. Physical mixtures (PMs) were also prepared and analysed.

4.5. Aerosol performance

The aerosolization performance was evaluated using an Andersen Cascade Impactor (ACI, Copley Scientific Ltd., UK) at 60 L/min airflow. Samples were filled in HPMC capsules and administered via a Breezhaler® device (Novartis AG, Switzerland) with a 4-second inhalation. Key aerodynamic parameters were calculated: MMAD (Mass Median Aerodynamic Diameter), FPF (Fine Particle Fraction), GSD (Geometric Standard Deviation), and EF (Emitted Fraction).

Also, Aerodynamic Particle Sizer (APS 3321; TSI Inc., Shoreview, MN, USA) was further used at same inputs used in ACI (4 s, 60 L/min). Three size-based parameters were analyzed: number particle size, surface particle size, and volume particle size.

Furthermore, *in silico* analysis using the latest Stochastic Lung Model (SLM) was employed, with inputs: 69.5 L/min, 1.7 L, and 2.04 s. Deposition fractions were expressed as lung deposition (bronchial + acinar), extra-thoracis, and exhaled percentage. Simulations also evaluated breath-hold effects at 5 and 10 s.

4.6. *In vitro* release study

A modified paddle method (Hanson SR8 Plus) using 100 mL vessels and mini paddles assessed KTP release in 50 mL simulated lung fluid (pH 7.4, 37 °C), at 50 rpm for 120 min. Aliquots (5 mL) were collected at set intervals and analyzed spectrophotometrically at 258 nm.

4.7. Viscosity measurement

Viscosity was assessed to evaluate potential effects on respiratory mucus properties. Type II mucin from porcine stomach (Sigma-Aldrich) was prepared at various concentrations, mixed with spray-dried samples, and stirred for 30 min. Viscosity was measured at 37 °C using a Rotavisk viscometer (IKA-Werke GmbH & Co. KG, Germany).

4.8. Anti-inflammatory effect

Anti-inflammatory activity was assessed using A549 (alveolar epithelial) and U937 (human pro-monocyte) cells (ATCC, Manassas, VA, USA). A549 cells were cultured in MEM and U937 cells in RPMI, both supplemented with 10% FBS, gentamicin, glucose, L-glutamine, and HEPES. Cells (1×10^6/well) were seeded into 6-well plates, treated with Lipopolysaccharides (LPS) and tested samples, and incubated (48 h at 37 °C with 5% CO_2).

4.9. Cell line measurements

Alveolar (A549) and bronchial (CFBE) cell lines were cultured at 37 °C with 5% CO_2. For co-culture, endothelial cells were seeded on the underside of collagen-coated 3 µm PET inserts, followed by A549 or CFBE on the upper side. Samples (0.5 mg/mL) were dispersed in culture medium or Ringer-HEPES. Cell viability was assessed via real-time impedance (RTCA-SP, ACEA Biosciences) after 48 h exposure to 50, 300, and 500 µg/mL. Permeability studies used 12-well inserts with Ringer-HEPES in donor (0.5 mL) and acceptor (1.5 mL) compartments. After 60 min shaking at 120 rpm, absorbance at 258 nm was measured to calculate apparent permeability (P_{app}), as per Equation 6.

$$P_{app}\ (cm/s) = \frac{\Delta[C]_A \times V_A}{A \times [C]_D \times \Delta t} \quad (6)$$

Transepithelial electrical resistance (TEER), marker molecule permeability assays, and immunocytochemistry were conducted to assess the integrity of intercellular junctions and confirm that barrier function remained intact post-permeability testing.

4.10. *In vivo* pharmacokinetics

Healthy 7-week-old male Sprague-Dawley rats (n = 48) were assigned to oral (n = 4/group) and inhalation (n = 20/group) groups. Oral groups received raw KTP (KTP-RAW) or nanosuspension (KTP-NS) via gavage, while inhalation groups received dry powders (K1 or K1ML) through intratracheal insufflation using a Penn-Century DP-4 device. All rats were dosed at 3 mg/kg. Blood and lung samples were collected at 15–360 min post-dose and analyzed by UHPLC-MS/HRMS (PRM mode). Pharmacokinetic parameters (C_{max}, T_{max}, $AUC_{0–6}$, $AUC_{0–\infty}$, k_e, $t_{½}$) were calculated using non-compartmental analysis in Phoenix WinNonlin (v8.5.2.4) with sparse sampling. Relative bioavailability (F) and tissue availability (f_t) were also determined as follows:

$$F\ (\%) = \frac{AUC_{0-\infty\ (intratracheal)}}{AUC_{0-\infty\ (Oral)}} \times \frac{Dose_{(oral)}}{Dose_{(intratracheal)}} \quad (7)$$

$$f_t = \frac{AUC_{0-6\ (lung)}}{AUC_{0-6\ (plasma)}} \quad (8)$$

4.11. Safety and tolerance in sensitized rats

Six-week-old male (n=24) and female (n=24) Wistar rats were sensitized by ovalbumin (OVA) to induce asthma-like conditions, then divided into five groups as follows: three OVA-sensitized and treated with K1, K1ML, or placebo (spray-dried stabilizer), one positive control (OVA-sensitized, untreated), and one negative control (non-sensitized, untreated). Intratracheal treatments were administered every third day (days 0–14) and every other day (days 14–21). The end-expiratory lung volume (EELV) was determined at positive end-expiratory pressure (PEEP) levels of 0, 3 and 6 cmH_2O. Airway resistance (Raw), tissue damping (G), and tissue elastance (H) were evaluated.

4.12. Stability study

Stability testing was conducted in a Binder KBF 240 chamber at 40 ± 2 °C/75 ± 5% relative humidity (RH) per ICH guidelines. Formulations placed in HPMC capsules were assessed over 3 months, with samples taken at 0, 1, and 3 months.

4.13. Statistical Analysis

GraphPad Prism 8.0.1 (CA, USA) was employed using a two-way ANOVA test, with significant values at $p \leq 0.05$. All data was expressed as mean ± SD.

5. Results and discussion

5.1. Nanosuspension characterization

Stabilizer effects were assessed via DLS. HPMC led to the largest PSs (~450–2570 nm) and highest PDIs, indicating poor stabilization. Compared to PVA, poloxamer 188 showed good zeta potential but larger particles. PVA at 1% (w/v) provided the smallest PS (238.3 ± 1.37 nm) and lowest PDI (0.082 ± 0.01) with ZP (−9.97 ± 5.31), therefore; it was selected.

NTA was used to provide more accurate size distribution, and results were as follows: D[0.1]: 119.60 ± 3.30 nm, D[0.5]: 168.70 ± 4.00 nm, D[0.9]: 230.80 ± 11.70 nm, with a span of 0.659 ± 0.024. A slight D[0.5] increase (+29 nm, $P \leq 0.001$) with stable span were recorded after holding time. Thus, the NS was deemed suitable for dry powder production.

5.2. Powder combinations for local pulmonary delivery assessments

5.2.1. QbD approach for combined DPI development

A flowchart outlines CF pathology and highlights the need for multi-drug inhaled therapies. Current treatments (e.g., TOBI®, Bronchitol®) target specific symptoms, while NSAIDs like KTP offer additional anti-inflammatory benefits. However, NSAID–mucolytic combinations remain unexplored. An Ishikawa diagram (Figure 1) mapped factors influencing the development of inhaled combinations, supporting QTPP definition for KTP–mannitol. Based on QTPP, key CQAs were identified (e.g., particle size, deposition, stability). Applying a QbD approach early in development improves efficiency, product quality, and regulatory outcomes.

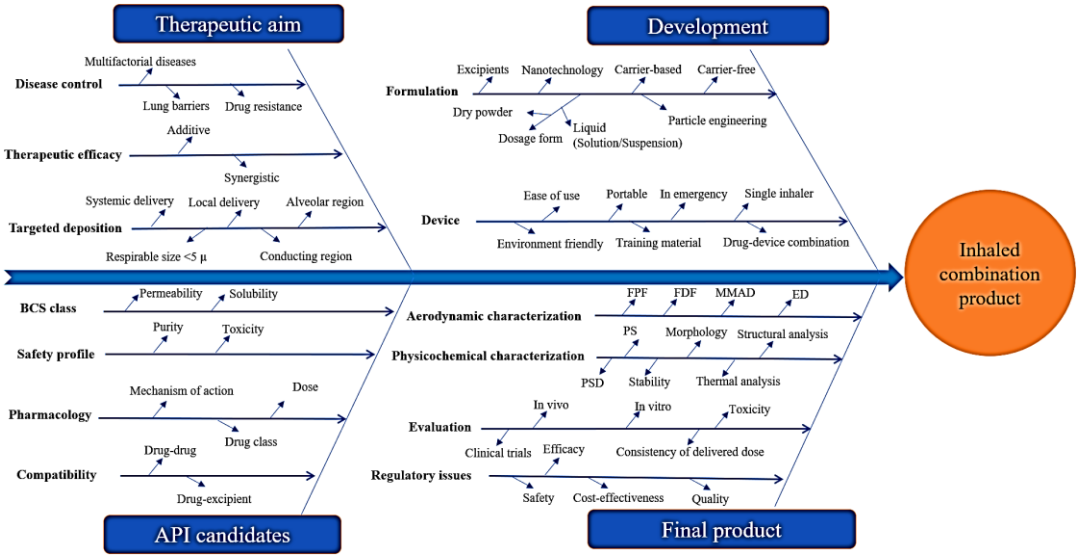

Figure 1: Fishbone diagram defining factors affecting the development of combined products for inhalation.

5.2.2. Powder characteristics

Table 2 confirms the effectiveness of our particle engineering, with spray drying maintaining KTP size (via DLS) and good redispersibility. Formulations had low tapped densities (0.18–0.22 g/cm³), suitable for inhalation, and yields of 53–59%, improved by higher mannitol levels reducing particle cohesion. Drug loading ranged from 57–85%, unaffected by mannitol concentration.

Table 2: Characteristics of spray-dried samples (F0-F2), including yield (%), drug loading (DL), particle size (DLS), density measurements, aerodynamic characteristics (ACI), and viscosity measurement.

Analysis	Parameter	F0	F0.5	F1	F2
Yield (%)	Yield (%)	52.95 ± 3.54	54.86 ± 6.12	57.29 ± 1.98	58.68 ± 9.73
Drug content	DL (%)	57.47 ± 1.44	84.12 ± 2.91	84.87 ± 7.13	84.72 ± 3.65
Particle size (DLS)	PS (nm)	204.9 ± 3.07	222.5 ± 4.11	240.7 ± 6.32	251.4 ± 2.84
	PDI	0.336 ± 0.003	0.127 ± 0.021	0.064 ± 0.008	0.156 ± 0.039
	ZP (mV)	−8.88 ± 0.27	−12.3 ± 0.43	−7.44 ± 0.18	−11.9 ± 0.33
Density	ρt (g/mL)	0.180 ± 0.002	0.192 ± 0.011	0.201 ± 0.009	0.228 ± 0.052
	ρb (g/mL)	0.124 ± 0.012	0.123 ± 0.003	0.120 ± 0.031	0.139 ± 0.024
Aerosol performance	MMAD (µm)	2.40 ± 0.17	2.80 ± 0.06	4.51 ± 0.41	4.90 ± 0.16
	FPF <5 (%)	56.16 ± 2.51	71.02 ± 1.19	64.32 ± 1.34	32.21 ± 3.67
	EF (%)	97.06 ± 3.22	96.60 ± 1.65	94.82 ± 2.79	95.70 ± 2.89
Rheology	Viscosity (Pa.s)	0.033 ± 1.98	0.031 ± 2.12	0.025 ± 1.37	0.030 ± 4.19

DLS: dynamic light scattering, PS: particle size, PDI: polydispersity index, ZP: zeta potential, ρt: tapped density, ρb: bulk density, MMAD: mass median aerodynamic size, FPF: fine particle fraction and EF: emitted fraction.

Figure 2 shows SEM images of spray-dried samples (F0–F2) with nearly spherical, rough-surfaced particles—ideal for pulmonary delivery and deposition. F0 had the smallest size, but increasing mannitol concentration (F0.5–F2) did not significantly alter particle size.

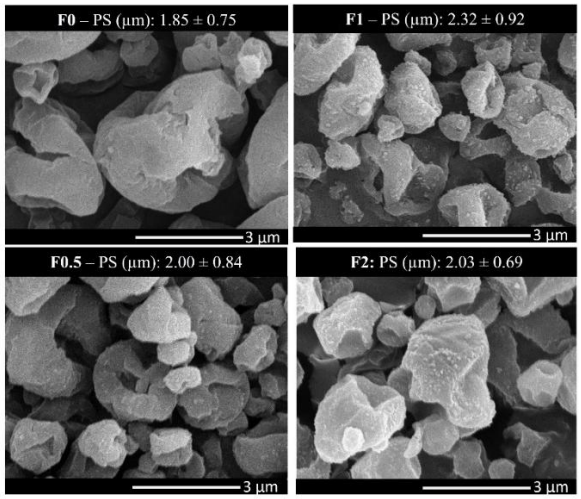

Figure 2: Morphology images using scanning electron microscope (SEM) of spray-dried samples with the diameter of final product measured by Image-J software. PS: particle size.

5.2.3. Solid-state analysis

DSC confirmed the crystalline nature of raw KTP (97.83 °C), with a melting point shift (~90 °C) in formulations indicating partial amorphization. Mannitol retained crystallinity (~152–156 °C), enhancing dissolution. Increased mannitol reduced KTP crystallinity, as shown by peak broadening in DSC and reduced XRPD intensity. XRPD revealed decreasing KTP crystallinity from 60.3% (F0) to 28.4% (F2). TGA showed low moisture content (1.08–2.12%), supporting good aerosolization.

5.2.4. *In vitro* aerosol performance (ACI)

All samples met EF criteria (95–97%) and showed high FPF (64–71%) (Table 2). F0.5 and F1 targeted deeper lung regions (ACI stages 3–4). High mannitol (F2) and mannitol-free (F0) samples showed more upper-airway deposition, confirming mannitol's concentration-dependent effect on deposition (Figure 3).

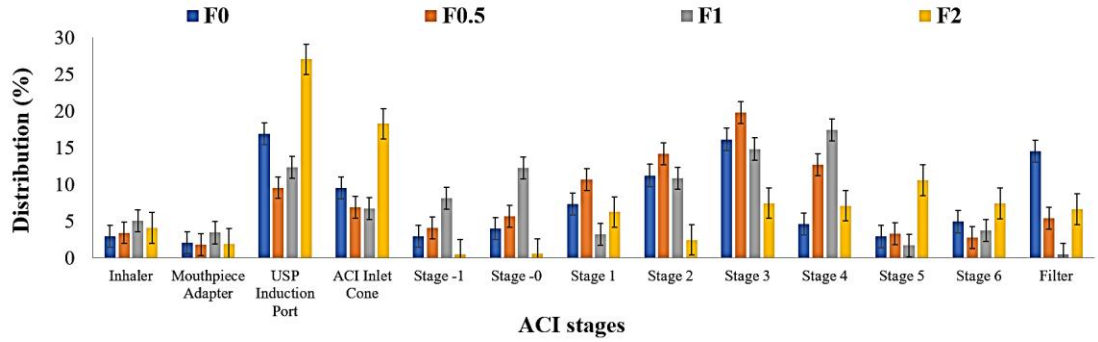

Figure 3: *In vitro* aerodynamic distribution of spray-dried samples at a flow rate of 60 L/min. Results are expressed as mean ± SD (n=3).

5.2.5. *In vitro* release study

Spray-dried samples showed fast release (~80% vs. 40% from PM in 5 min). F1 showed the fastest release (~100% in 10 min), while suboptimal mannitol levels (F0.5, F2) reduced this effect, highlighting the need for optimized ratios.

5.2.6. Viscosity measurement

Only F1 slightly reduced 10% mucin viscosity (0.035 Pa·s), suggesting optimal mannitol concentration promotes mucus thinning—important for CF treatment (Table 2). Thus, F1 was selected for further studies, with F0 serving as a reference.

5.2.7. Anti-inflammatory effect

In LPS-stimulated U937 cells, all formulations significantly reduced IL-6 without mannitol interference; no effect was seen in A549 cells, consistent with literature (Figure 4). This supports the anti-inflammatory potential of KTP–mannitol combinations.

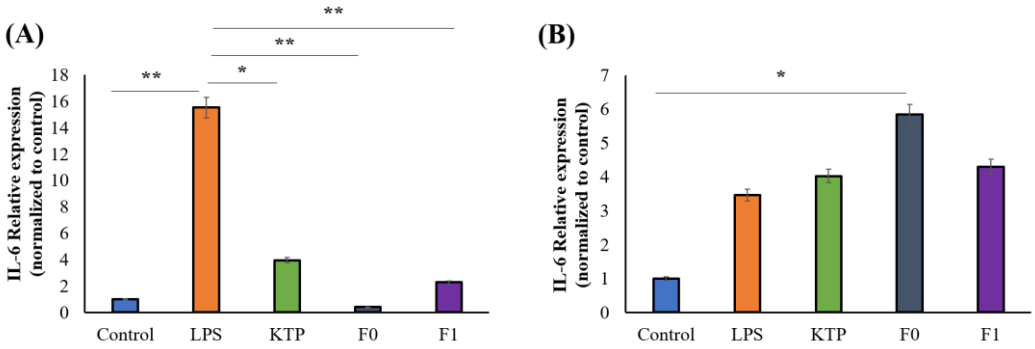

Figure 4: Relative expression of IL-6 on two cell lines; (**A**) U937 and (**B**) A549. Control is the untreated cell line, LPS is the treated cell line, raw KTP, F0, F0.5, F1 and F2 are treated with LPS. Results are expressed as mean ± SD (n=3). Level of significance: *p < 0.05, **p < 0.01.

5.2.8. Cell line evaluation

Viability*:* F0 and F1 were well tolerated by A549 and CFBE cells, with minor impedance drop only at high F1 concentrations in A549.

Permeability*:* F1 improved KTP transport across A549 by 1.4-fold, likely due to mannitol's effect on particle surface (Figure 5). **Barrier integrity** was also maintained, confirming the safety and efficacy of the combination DPI for lung delivery.

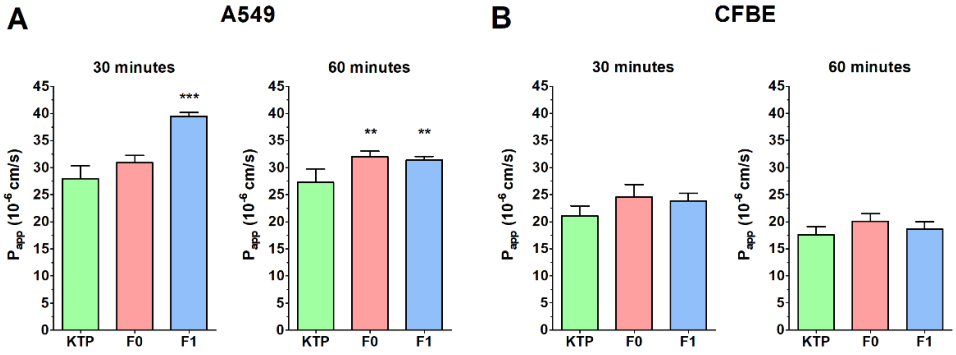

Figure 5: Permeability of raw KTP, F0, and F1 (50 µg/mL KTP concentration in the donor compartment) across the co-culture model of (**A**) alveolar epithelial cells and (**B**) bronchial epithelial cells after 30- and 60-min assay time. Values are presented as means ± SD, n = 4. ** p < 0.01, *** p < 0.001.

5.3. Nanocrystal-based dry powder for systemic delivery evaluations

5.3.1. Factorial design

A BBD optimized nano spray-drying by varying pump rate, temperature, and feed concentration over 15 runs, with responses visualized in 3D surface plots (Figure 6). Key inhalation parameters —D[0.5] and span—guided the optimization. Higher pump rates reduced size and span; high feed concentrations increased size; low concentrations caused higher spans. At 90 °C, particles were smaller and more uniform, while 100–110 °C led to aggregation. Optimal settings (50% pump, 90 °C, 5% feed) were chosen for mannitol/leucine-based NCA formulations.

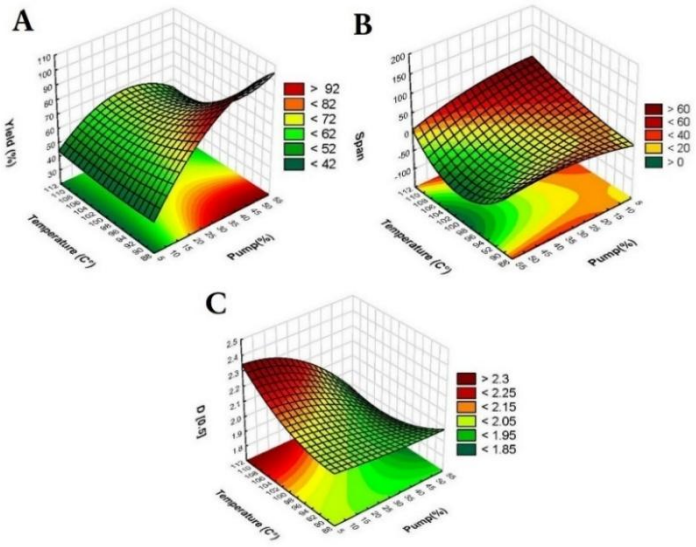

Figure 6: 3D surface plots of the effect of temperature (°C) and pump (%) on (**A**): yield (%), (**B**): span and (**C**): D[0.5].

5.3.2. Powder characteristics

Following process optimization, all formulations showed D[0.5] values between ~1.7 and 3.3 µm. Leucine slightly increased particle size (due to droplet stabilization), while mannitol caused the largest sizes due to its crystallinity after spray drying. Combined (K1ML), they produced intermediate sizes and narrower span values, suggesting improved uniformity and lung deposition potential. Powder densities were suitable for inhalation (bulk <0.3 g/mL), with K1ML offering favorable density for deep lung delivery. Drug loading (DL) and encapsulation efficiency (EE) were highest in K1; leucine improved EE, while both excipients slightly reduced DL (Table 3).

Table 3: Characteristics of NCAs, including particle size (laser diffraction), drug loading (DL), encapsulation efficiency (EE), density measurements, and aerodynamic performance (ACI).

Analysis	Parameter	K1	K1M	K1L	K1ML
Particle size	D[0.5]	1.708 ± 0.074	3.337 ± 0.190	1.893 ± 0.017	2.046 ± 0.064
	span	1.412 ± 0.071	1.390 ± 0.118	1.372 ± 0.070	1.387 ± 0.008
	SSA (m^2/g)	3.945 ± 0.247	2.09 ± 0.156	3.56 ±0.001	3.290 ± 0.057
Drug content	DL (%)	41.38 ± 3.54	26.24 ± 6.12	30.08± 1.98	20.55 ± 9.73
	EE (%)	84.83 ± 1.44	80.04 ± 2.91	91.73 ± 7.13	83.24 ± 3.65
Density	ρt (g/mL)	0.225	0.097	0.225	0.34
	ρb (g/mL)	0.144	0.064	0.144	0.189
Aerosol performance	MMAD (µm)	2.016 ± 0.17	4.50 ± 0.06	0.927 ± 0.41	2.661 ± 0.16
	FPF <5 (%)	84.07 ± 1.51	25.05 ± 1.19	89.96 ± 1.34	69.30 ± 3.67
	FPF <3 (%)	74.73 ± 1.23	20.65 ± 1.91	79.88 ± 1.42	52.75 ± 1.57
	EF (%)	95.56 ± 3.22	97.05 ± 1.65	96.23 ± 2.79	92.67 ± 2.89
	GSD	1.658	2.95	N/A	1.986

SEM images showed K1 as nanocrystals on the stabilizer surface, K1L with a corrugated shell (due to leucine), K1M as larger rough spheres (mannitol effect), and K1ML combining both traits. All samples had rough surfaces, which aid lung deposition via improved cell attachment (Figure 7).

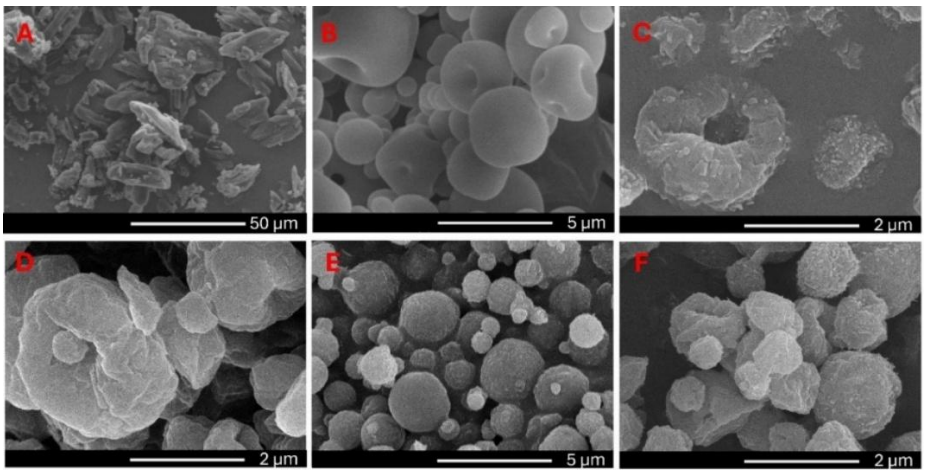

Figure 7: SEM images of (**A**) raw KTP, (**B**) nano spray dried-stabilizer system, (**C**) K1, (**D**) K1L, (**E**) K1M and (**F**) K1ML.

5.3.3. Solid-state analysis

DSC and TGA revealed reduced KTP melting points and low moisture content (<2%), with mannitol polymorphism noted in K1ML. XRPD showed retained crystallinity, highest in K1L, lowest in K1M. FTIR confirmed structural integrity, with mannitol and leucine altering hydrogen bonding in PVA, indicating molecular-level interactions.

5.3.4. Aerosol performance

ACI data confirmed MMADs between 0.9–4.5 µm, suitable for lung deposition. K1L had high FPF but with exhalation risk due to low MMAD (<1 µm); K1M had broader size distribution. K1ML balanced FPF and MMAD, favoring deep lung delivery (Table 3). APS results aligned with ACI. *In silico* models supported these trends—K1ML achieved optimal lung targeting. Extended breath-holds further improved deposition.

5.3.5. *In vitro* release study

Rapid drug release (>93% in 5 min) was observed for all formulations, highest for K1ML (~99% in 5 min). PM released only 40%. Faster release was linked to smaller size, surface roughness, and excipient effects on wettability and dispersion, consistent with prior studies (Figure 8). Hence, K1ML was selected for further study, with K1 as reference.

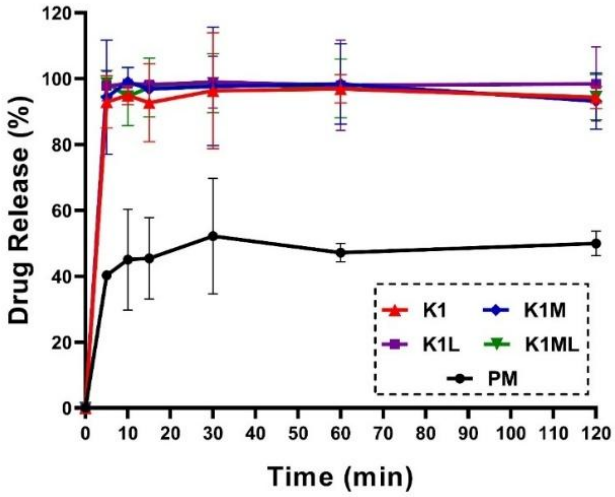

Figure 8: In vitro release study of physical mixture (PM) and developed NCAs (K1, K1M, K1L, and K1ML) in simulated lung media (SLM). Results are expressed as mean ± SD (n=3).

5.3.6. Cell line measurements

Viability: No significant cytotoxicity was observed in CFBE; A549 showed slight impedance reduction at high concentrations. A safe concentration of 50 µg/mL was selected for further assays. **Permeability**: KTP and NCA formulations (K1, K1ML) showed efficient permeability. K1ML slightly enhanced A549 permeability. Neither significantly altered permeability compared to raw KTP, suggesting that the engineered NCAs enhanced solubility and dissolution of KTP without negatively influencing epithelial permeability. **Barrier Integrity**: It was confirmed by TEER values (unchanged), and by immunostaining of ZO-1 (CFBE) and β-catenin (A549), with no morphological changes (Figure 9).

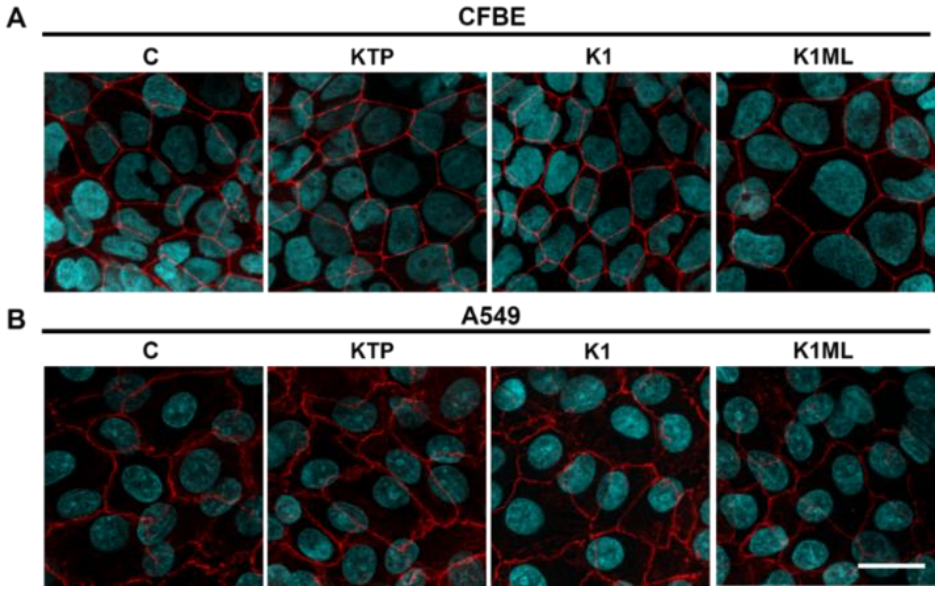

Figure 9: Barrier integrity assessed by immunostaining in (**A**) CFBE cells (ZO-1 staining) and (**B**) A549 cells (β-catenin staining) after permeability. Cyan: cell nuclei; red: junctional proteins. Bar = 20 µm.

5.3.7. Pharmacokinetic study in healthy rats

K1ML showed superior systemic exposure (779.9% bioavailability vs. KTP-RAW), outperforming KTP-NS and K1 (Figure 10).

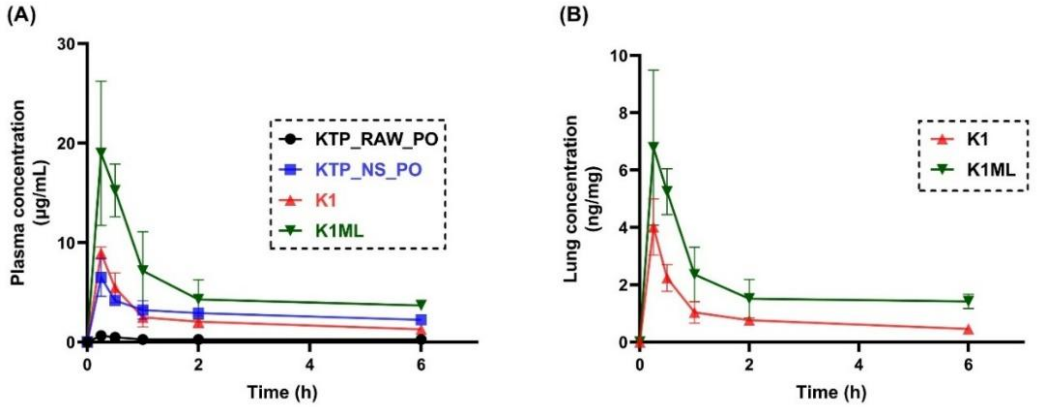

Figure 10: The concentration-time curve of KTP (**A**) in plasma after oral administration of KTP-raw and KTP-NS and intratracheal administration of K1 and K1ML, (**B**) in lungs after intratracheal administration of K1 and K1ML. Administered dose was 3 mg KTP/kg. Data are expressed as mean ± SD (n = 4).

Inhalation improved C_{max} and AUC compared to oral KTP-NS. Lung KTP levels remained low (low f_t values), with K1ML offering longer systemic exposure (significantly greater $AUC_{0-\infty}$ and 1.7-fold higher absorption vs. KTP-NS) (Table 4). This supports the potential of inhaled delivery for enhanced bioavailability systemically.

Table 4: The pharmacokinetic parameters of KTP obtained from both plasma and lung concentration-time curves by non-compartmental analysis after oral administration of KTP-RAW and KTP-NS, and intratracheal administration of NCA formulations (K1 and K1ML), (Mean ± SD, n = 4).

	PK parameter	KTP-RAW	KTP-NS	K1	K1ML
Plasma	k_e (h−1)	0.0653 ± 0.0423	0.0919 ± 0.0164	0.1269[a]	0.1366[a]
	$t_{½}$ (h)	21.306 ± 4.509	7.720 ± 1.354[a]	5.460[a]	5.072[a]
	t_{max} (h)	0.25	0.25	0.25	0.25
	C_{max} (μg/mL)	0.646 ± 0.098	6.499 ± 1.9122	8.949 ± 0.611[a]	18.973 ± 7.246[a,b,c]
	$AUC_{0-\infty}$ (μg·h/mL)	9.329 ± 8.897	42.163 ± 3.150[a]	24.125[a,b]	72.763[a,b,c]
	F (to KTP_RAW)	-	4.519	2.586	7.799
	F (to KTP_NS)	0.221	-	0.572	1.726
Lung	k_e (h−1)	-	-	0.1535	0.1671
	$t_{½}$ (h)	-	-	4.515	4.147
	t_{max} (h)	-	-	0.25	0.25
	C_{max} (μg/mg)	-	-	0.00402 ± 0.00803	0.00678 ± 0.0136
	$AUC_{0-\infty}$ (μg·h/mg)	-	-	0.00843	0.02037
	f_t	-	-	0.0003912	0.0003241

[a]: indicates statistically significant difference from KTP-RAW ($P < 0.05$). [b]: indicates statistically significant difference from KTP-NS ($P < 0.05$). [c]: indicates statistically significant difference from K1 ($P < 0.05$).

5.3.8. Safety and tolerance in ovalbumin-sensitized rats

PEEP-adjusted lung mechanics showed increased EELV and Raw in K1ML, indicating airway narrowing (Figure 11). This may be due to higher bioavailability (elevated systemic COX inhibition) or excipient effects. Literature suggests mannitol can cause bronchoconstriction at high doses. Future studies should explore dose reduction and bronchodilator co-delivery.

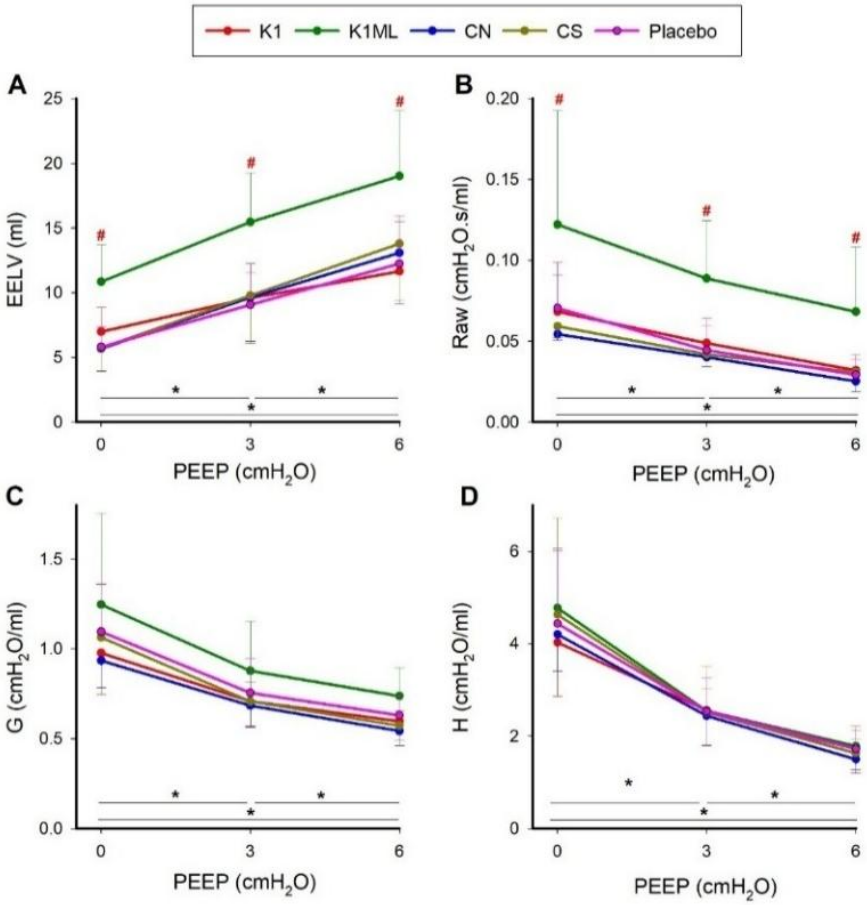

Figure 11: Lung function parameters in OVA-sensitized rats across varying PEEP levels: (**A**) End-expiratory lung volume (EELV), (**B**) airway resistance (Raw), (**C**) respiratory tissue damping (G) and (**D**) respiratory tissue elastance (H). Where *: $p<0.05$ for PEEP change in all groups and #: $p<0.05$ K1ML vs. other groups.

5.4. Stability assessment of selected samples

After 3 months under stress, F1 showed increased span, reduced FPF, and slower release—likely due to solid-state changes and particle interactions. In contrast, K1ML maintained D[0.5], span, and MMAD, though FPF slightly declined, possibly from surface moisture effects. Despite this, drug release and thermal behavior remained stable, indicating acceptable shelf-life performance. Further studies should address moisture sensitivity.

6. Conclusion

This dissertation employed a patient-centric strategy to address distinct therapeutic needs—local and systemic—through pulmonary delivery using KTP-based DPIs. Two formulations were developed from a unified nanocrystal platform: one designed to treat lung inflammation and mucus obstruction in CF, and the other optimized for systemic delivery with enhanced bioavailability. The main findings, organized according to the defined objectives, are summarized as follows:

A. Nanocrystal dispersion preparation

I. A stable nanocrystal suspension was successfully optimized using 1% PVA and 0.1% SDS. Over 45 days of refrigerated storage, only minimal particle size growth was observed, while size distribution remained consistent, qualifying the dispersion for downstream solidification and engineering.

B. Local pulmonary delivery (nanocrystal KTP-mannitol combination therapy)

II. A QbD framework supported the rationale for combining KTP with mannitol in a single inhaler to address both inflammation and mucus accumulation in CF, aiming to improve disease control and patient quality of life.

III. The optimized formulation (F1; containing KTP and mannitol in 1:1 mass ratio, with 84.9% DL) demonstrated efficient aerosol performance, with deposition primarily in ACI stages 3 and 4, confirming desired lung delivery. It achieved complete drug release (~100%) within 10 minutes in simulated lung fluid, notably reduced mucin viscosity without compromising KTP's anti-inflammatory effect, and showed good biocompatibility in alveolar and bronchial cells. A 1.4-fold increase in alveolar permeability was achieved. However, deviations from the 1:1 ratio (either higher or lower) negatively impacted performance.

IV. These findings highlight the formulation’s potential as a dual-function inhalable therapy for CF, though precise mannitol concentration remains critical to maintaining efficacy and performance. This novel inhaled combination supports patient-centric delivery by reducing doses burden, improving symptom control, and enhancing adherence

C. Systemic pulmonary delivery (nanocrystal-engineered DPI)

V. A factorial design (BBD) optimized nano spray-drying parameters (50% pump rate, 5% (w/v) feed concentration and 90 °C inlet temperature), enabling the production of KTP engineered-nanocrystal agglomerates tailored for systemic absorption via the deep lung deposition.

VI. The inclusion of both mannitol and leucine demonstrated a synergistic effect on particle engineering, significantly enhancing aerosol behavior and dispersion compared to formulations with either excipient alone. The optimized mannitol-leucine formulation (K1ML; containing 2.5% KTP, 1.25% mannitol and 1.25% leucine (w/v)) achieved excellent *in vitro* aerosol performance (MMAD: 2.66 ± 0.16 μm; FPF: 69.3 ± 3.67%) and complete drug release (99% in 5 min). It also maintained biocompatibility across both CFBE and A549 cells, with greater permeability in alveolar cells.

VII. Pharmacokinetic evaluation of inhaled K1ML confirmed a 3-fold increase in C_{max} and 1.73-fold improvement in relative bioavailability (73% for K1ML vs. 42% for oral KTP-NS). Low lung tissue retention indicated efficient systemic absorption, supporting its suitability for extra-pulmonary indications and rapid systemic absorption. However, repeated dosing in an OVA-sensitized rat model revealed bronchial side effects (e.g., airway narrowing and reduced expiratory flow) for K1ML, indicating that dose adjustment is required to balance efficacy and pulmonary safety. The nanocrystal-engineered DPI system aligns with patient-centric goals by improving bioavailability, reducing gastrointestinal-related side effects, accelerating therapeutic onset, and potentially lowering dosing frequency.

D. Stability assessment

VIII. Over three months of ICH storage (40°C/75% RH), F1 exhibited a broadened particle size distribution (span), reduced FPF, and a compromised release profile, indicating the need for further optimization of mannitol concentration or incorporation of an additional stabilizing agent. In contrast, K1ML maintained its particle size, MMAD, and *in vitro* release characteristics, demonstrating robust stability and greater suitability for potential commercial development.

7. Novelty and practical relevance of the work

The main innovations and practical contributions of this study include:

- First application of a unified KTP nanocrystal suspension engineered to serve both local and systemic delivery via inhalable powders, developed using a patient-centric strategy.
- Novel QbD-driven Zero Phase formulation rationale proposed for a DPI combination therapy in CF, supporting dual functionality—anti-inflammatory action (via KTP) and mucus hydration (via mannitol).
- First demonstration of mannitol–leucine synergy in enhancing aerosolization, cellular permeability, and systemic bioavailability of a nanocrystal-engineered DPI.
- Development of the first NSAID-based DPI intended specifically for systemic absorption, offering a needle-free alternative to injectable and oral routes.
- First-time comprehensive assessment of potential respiratory risks associated with prolonged inhaled NSAID (KTP) use, using an OVA-sensitized rat model to evaluate lung function and airway mechanics in an asthmatic-like condition.
- Integration of KTP and mannitol in a single DPI formulation to address polytherapy needs in CF, by targeting inflammations and mucus overproduction simultaneously, aiming to improve adherence and simplify treatment.
- Implementation of a scalable and clinically relevant spray-drying process aligned with patient usability and regulatory trends in patient-focused drug design.
- Advancement of pulmonary drug delivery as a route for repurposing poorly soluble drugs, with potential for broad application to other therapeutic classes such as antivirals or immunomodulators.
- Supports regulatory interest in IVIVC and patient-centricity by demonstrating rational formulation design tied to improved therapeutic performance and usability.
- These innovations represent an important shift toward more effective and patient-aligned therapies.

PUBLICATIONS RELATED TO THE SUBJECT OF THE THESIS

I. **Heba Banat**, Rita Ambrus, Ildikó Csóka, “Drug combinations for inhalation: Current products and future development addressing disease control and patient compliance”. International Journal of Pharmaceutics. 2023; 643:123070. https://doi.org/10.1016/j.ijpharm.2023.123070

(**D1, IF: 5.3**)

II. **Heba Banat**, Ildikó Csóka, Dóra Paróczai, Katalin Burian, Árpád Farkas, Rita Ambrus. “A Novel Combined Dry Powder Inhaler Comprising Nanosized Ketoprofen-Embedded Mannitol-Coated Microparticles for Pulmonary Inflammations: Development, In Vitro–In Silico Characterization, and Cell Line Evaluation”. Pharmaceuticals. 2024; 17(1):75. https://doi.org/10.3390/ph17010075

(**Q1, IF: 4.3**)

III. **Heba Banat,** Ilona Gróf, Mária A. Deli, Rita Ambrus, Ildikó Csóka. “Evaluation of Permeability, Safety, and Stability of Nanosized Ketoprofen Co-Spray-Dried with Mannitol for Carrier-Free Pulmonary Systems”. Applied Sciences. 2025; 15(3):1547. https://doi.org/10.3390/app15031547

(**Q2, IF: 2.5**)

IV. **Heba Banat**, Attila Nagy, Árpád Farkas, Rita Ambrus, Ildikó Csóka. “Comprehensive Aerodynamic and Physicochemical Stability Evaluations of Nanocrystal-Based Dry Powder Inhalers: The Role of Mannitol and Leucine in Enhancing Performance”. Pharmaceutics. 2025; 17(4), 436. https://doi.org/10.3390/pharmaceutics17040436

(**D1, IF: 4.9**)

V. **Heba Banat**, Ildikó Csóka, Fruzsina Kun-Szabó, Gergely H. Fodor, Petra Somogyi, Ferenc Peták, Petra Party, Anita Sztojkov-Ivanov, Eszter Ducza, Róbert Berkecz, Ilona Gróf, Mária A. Deli, Rita Ambrus. “Mannitol-leucine synergy in nanocrystal agglomerates for enhanced systemic delivery of inhaled ketoprofen: Pharmacokinetics and safety in ovalbumin-sensitized rats”. International Journal of Pharmaceutics. 2025; 676:125610. https://doi.org/10.1016/j.ijpharm.2025.125610

(**Q1, IF: 5.3**)

Total IF: **22.3**, Total citation: **30**

PRESENTATIONS RELATED TO THE SUBJECT OF THE THESIS

I. **Heba Banat**, Ildikó Csóka, Rita Ambrus, "Formulation of a combined dry powder inhalation therapy for cystic fibrosis". IV. Symposium of Young Researchers on Pharmaceutical Technology, Biotechnology and Regulatory Science. January 19-21, 2022. Szeged, Hungary. Flash Presentation.

II. **Heba Banat**, Ildikó Csóka, Rita Ambrus, "Development of a combined nanosystem as a dry powder inhaler for the treatment of pulmonary inflammations". V. Symposium of Young Researchers on Pharmaceutical Technology, Biotechnology and Regulatory Science. January 18-20, 2023. Szeged, Hungary. Oral Presentation.

III. **Heba Banat**, Ildikó Csóka, Rita Ambrus, "Design, formulation and evaluation of a dry powder inhaler comprising a combination therapy to target chronic respiratory diseases". EUFEPS Annual Meeting 2023. May 31 – June 2, 2023, Lisbon, Portugal. Poster presentation.

IV. **Heba Banat**, Ildikó Csóka, Rita Ambrus, "Optimizing Aerodynamic Performance of an Anti-Inflammatory-Containing Dry Powder Inhaler via Nano-Spray Drying". VI. Symposium of Young Researchers on Pharmaceutical Technology, Biotechnology and Regulatory Science. January 24-26, 2024. Szeged, Hungary. Oral Presentation.

V. **Heba Banat**, Ildikó Csóka, Dóra Paróczai, Katalin Burian, Árpád Farkas, Rita Ambrus, "Development and formulation of a single dry powder inhaler combining ketoprofen nanoparticles-embedded mannitol microparticles for pulmonary inflammations: in vitro and in silico analysis, and cell line assessment". XVI. Hungarian Aerosol Conference. 2024. April 25-27, 2024 - Szarvas, Hungary. Oral Presentation.

VI. **Heba Banat**, Ildikó Csóka, Rita Ambrus, "Enhancing Pulmonary Delivery of Ketoprofen: Comparative Study of Spray Drying Approaches". Exploring the Future of Inhalation Drug Delivery. September 11-13, 2024. Parma, Italy. Oral Presentation.

VII. **Heba Banat**, Ildikó Csóka, Rita Ambrus, "Carrier-Free Dry Powder Inhaler Formulation for Pulmonary Delivery: Insights into Stability, Safety, and Aerodynamic Performance". VII. Symposium of Young Researchers on

Pharmaceutical Technology, Biotechnology and Regulatory Science. January 29-31, 2025. Szeged, Hungary. Oral Presentation.

VIII. **Heba Banat**, Rita Ambrus, Ildikó Csóka, "Enhancing Bioavailability of a Non-Steroidal Anti-Inflammatory Drug Through Pulmonary Delivery". Drug Delivery Through Physiological Barriers. International Symposium April 24-26, 2025. Budapest, Hungary. Oral Presentation.

Acknowledgement

I would like to express my sincere gratitude to the Head of the Institute and my supervisor, **Prof. Dr. Ildikó Csóka**, for fostering a supportive environment and for cultivating a diverse scientific culture at our Institute. My deepest appreciation goes to my co-supervisor, **Prof. Dr. Rita Ambrus**, for her constant encouragement, rigorous scientific mentorship, and unwavering support throughout my PhD journey. I consider myself deeply fortunate to have had her as a mentor.

I would like to acknowledge all my co-authors and collaborators: **Dr. Árpád Farkas** (Institute for Energy Security and Environmental Safety, HUN-REN Centre for Energy Research); **Dr. Dóra Paróczai** and **Prof. Dr. Katalin Burián** (Department of Medical Microbiology, University of Szeged); **Dr. Ilona Gróf** and **Prof. Dr. Mária A. Deli** (Institute of Biophysics, HUN-REN Biological Research Centre); **Fruzsina Kun-Szabó**, **Dr. Gergely H. Fodor**, **Petra Somogyi**, and **Prof. Dr. Ferenc Peták** (Department of Medical Physics and Informatics, University of Szeged); **Dr. Anita Sztojkov-Ivanov** and **Dr. Eszter Ducza** (Institute of Pharmacodynamics and Biopharmacy, University of Szeged); **Dr. Róbert Berkecz** (Institute of Pharmaceutical Analysis, University of Szeged); **Dr. Petra Party** (Institute of Pharmaceutical Technology and Regulatory Affairs, University of Szeged); and **Dr. Attila Nagy** (Wigner Research Centre for Physics, Hungarian Academy of Sciences). Also, special thanks are extended to **Erika Feczkóné Boda**, **Klára Kovács**, and **Balázs Béniám** for their technical assistance.

This work was financially supported by **Tempus Public Foundation** through the **Stipendium Hungaricum Program** (Registry no. **SHE-40702-004/2021**). Further support was provided by the **NKFIH OTKA K_146148 project** and **Project No. TKP2021-EGA-32**.

Finally, I am eternally grateful to my father, **Fayez**, whose steadfast emotional and financial support has been a cornerstone of this journey, and to my beloved mother, **Intisar**, whose endless love, care, and prayers have been a constant source of strength and comfort. My deepest thanks go also to my cherished siblings—**Dr. Mahmoud**, **Haneen**, **Dr. Hadeel**, **Hayat**, and **Lamar**—for their unconditional love and understanding throughout my studies. I am forever grateful to those **dear souls** who never leave us—their presence a constant strength, far beyond any distance.

Above all, I thank **Allah** for granting me the strength, patience, and resilience to complete this journey. Every success I have achieved is by His will and grace, "الحمدلله".